# Genetic suppression of defective profilin by attenuated Myosin II reveals a potential role for Myosin II in actin dynamics in vivo in fission yeast

Paola Zambon[a], Saravanan Palani[a], Shekhar Sanjay Jadhav[b], Pananghat Gayathri[b], and Mohan K. Balasubramanian[a,*]

[a]Division of Biomedical Sciences, Warwick Medical School, University of Warwick, Coventry CV4 7AL, United Kingdom; [b]Biology Division, Indian Institute of Science Education and Research, Pune, Maharashtra 411008, India

**ABSTRACT** **The actin cytoskeleton plays a variety of roles in eukaryotic cell physiology, ranging from cell polarity and migration to cytokinesis. Key to the function of the actin cytoskeleton is the mechanisms that control its assembly, stability, and turnover. Through genetic analyses in *Schizosaccharomyces pombe*, we found that *myo2*-S1 (*myo2*-G515D), a Myosin II mutant allele, was capable of rescuing lethality caused by partial defects in actin nucleation/stability caused, for example, through compromised function of the actin-binding protein Cdc3-profilin. The mutation in *myo2*-S1 affects the activation loop of Myosin II, which is involved in physical interaction with subdomain 1 of actin and in stimulating the ATPase activity of Myosin. Consistently, actomyosin rings in *myo2*-S1 cell ghosts were unstable and severely compromised in contraction on ATP addition. These studies strongly suggest a role for Myo2 in actin cytoskeletal disassembly and turnover in vivo, and that compromise of this activity leads to genetic suppression of mutants defective in actin filament assembly/stability at the division site.**

**Monitoring Editor**
Laurent Blanchoin
CEA Grenoble

Received: Apr 6, 2020
Revised: Jun 24, 2020
Accepted: Jun 25, 2020

## INTRODUCTION

Actin is a highly conserved cytoskeletal polymer that exists as monomers and filamentous structures that are important for a vast array of physiological processes in the living world. In eukaryotes, the actin cytoskeleton plays essential roles in cell polarity, migration, and cytokinesis (Pollard and Wu, 2010; Cheffings *et al.*, 2016; Misu *et al.*, 2017; Rottner *et al.*, 2017; Skruber *et al.*, 2018). A balance of factors that control filament nucleation and stability and those that promote its disassembly regulates the functions of the actin cytoskeleton (Lee and Dominguez, 2010). Over the past three decades, the fission yeast *Schizosaccharomyces pombe* has emerged as an attractive organism for the study of the actin cytoskeleton and its role in cell polarity and division (Pollard and Wu, 2010; Cheffings *et al.*, 2016; Chiou *et al.*, 2017). This is particularly due to the fact that many of the actin cytoskeletal proteins can be characterized through easily identifiable mutant phenotypes (Wertman *et al.*, 1992; Holtzman *et al.*, 1994; McCollum *et al.*, 1996; Bezanilla *et al.*, 1997; Kitayama *et al.*, 1997; May *et al.*, 1997; Motegi *et al.*, 1997; Balasubramanian *et al.*, 1998; Wu *et al.*, 2001; Nakano and Mabuchi, 2006). Work in *Saccharomyces cerevisiae* has also helped define a number of phenotypes indicative of actin cytoskeletal defects (Wertman *et al.*, 1992; Holtzman *et al.*, 1994).

In fission yeast, actin exists in three types of structures: actin patches, which are nucleated by the Arp2/3 complex (Pelham and Chang, 2001; Sirotkin *et al.*, 2010); linear interphase actin cables, nucleated by the formin-For3 (Feierbach and Chang, 2001); and the cytokinetic actomyosin ring (AMR), nucleated by the formin-Cdc12 (Chang *et al.*, 1997) and the actin-binding protein Cdc3-profilin (Balasubramanian *et al.*, 1994). The coiled-coil actin-binding protein Cdc8-tropomyosin ensures stability of actin cables and AMR (Liu and Bretscher, 1989; Balasubramanian *et al.*, 1992; Gunning *et al.*, 2015). The fission yeast actin cytoskeleton undergoes dramatic disassembly and turnover (Kovar *et al.*, 2011). Treatment of cells with the actin polymerization inhibitor Latrunculin A (LatA) causes complete loss of actin cables, AMRs,

This article was published online ahead of print in MBoC in Press (http://www.molbiolcell.org/cgi/doi/10.1091/mbc.E20-04-0224) on July 2, 2020.

*Address correspondence to: Mohan K. Balasubramanian (m.k.balasubramanian@warwick.ac.uk).

Abbreviations used: AMR, actomyosin ring; CW, Calcofluor white; DAPI, 4′,6-diamidino-2-phenylindole; Jasp, Jasplakinolide; LatA, Latrunculin A; PBS, phosphate-buffered saline; YES, yeast extract medium.

and actin patches (in that order) (Pelham and Chang, 2001, 2002). While the actin severing protein Adf1 (cofilin) plays a key role in actin cytoskeletal disassembly (Nakano and Mabuchi, 2006; Pavlov *et al.*, 2007), the fact that the actin cables and rings still turn over, albeit slowly, in *adf1*-1 mutants (Nakano and Mabuchi, 2006) suggests that other mechanisms should also exist to disassemble the actin cytoskeleton. The actin cytoskeleton is also modulated by the Adf1-related Gmf1 protein in fission yeast (Nakano *et al.*, 2010). Myosin-family proteins have also been shown to destabilize the actin cytoskeleton in plants and metazoa (Staiger *et al.*, 2009; Murrell and Gardel, 2012; Henty-Ridilla *et al.*, 2013; Vogel *et al.*, 2013; Cai *et al.*, 2014), although genetic evidence to this effect is scarce.

Myo2-S1 (Myo2 G515D) was isolated in a genetic screen for suppressors of the high temperature lethality of *cdc3*-124 that led to characterization of the Arp2/3 complex protein Sop2 (Balasubramanian *et al.*, 1996; Wong *et al.*, 2000), although Myo2-S1 mutant has not been previously characterized. Here we characterize the cellular and molecular basis of the suppression of *cdc3*-124 and other conditions that cause partial loss of the actin cytoskeleton. These studies point to an in vivo role for Myosin II in actin filament disassembly.

## RESULTS AND DISCUSSION

### *myo2*-S1 suppresses the ts lethality of *cdc3*-124

Previous work has shown that *cdc3*-124 is defective in AMR assembly and colony formation above 32°C (Balasubramanian *et al.*, 1996). To investigate the suppression of *cdc3*-124 by *myo2*-S1, we freshly generated *cdc3*-124 *myo2*-S1 from a cross between a *myo2*-S1 parent (obtained after three back crosses) and *cdc3*-124. This *cdc3*-124 *myo2*-S1 strain was compared with wild-type, *cdc3*-124, and *myo2*-S1. As expected, wild-type formed colonies at all temperatures tested, whereas *cdc3*-124 failed to form colonies at and above 32°C (Figure 1A). *myo2*-S1 was able to form colonies at all temperatures tested, although these cells displayed cytokinesis defects at all temperatures (described in later sections) (Figure 1A). Importantly, *cdc3*-124 *myo2*-S1 was able to form colonies at 34°C and did so poorly, even at 36°C (Figure 1A). We found that *cdc3*-124 *myo2*-S1 was sicker than *myo2*-S1, although this double mutant was healthier than *cdc3*-124 and hence the observed genetic suppression. The genetic screen (Balasubramanian *et al.*, 1996) also identified a different suppressor allele of *myo2*, *myo2*-S2 (Myo2 E679K) (Wong *et al.*, 2000) (Figure 1A). We recreated the *cdc3*-124 *myo2*-S2 and found that it rescued *cdc3*-124 at 34°C, but barely at 36°C (Figure 1A). The well-characterized *myo2*-E1 (Balasubramanian *et al.*, 1998) did not rescue

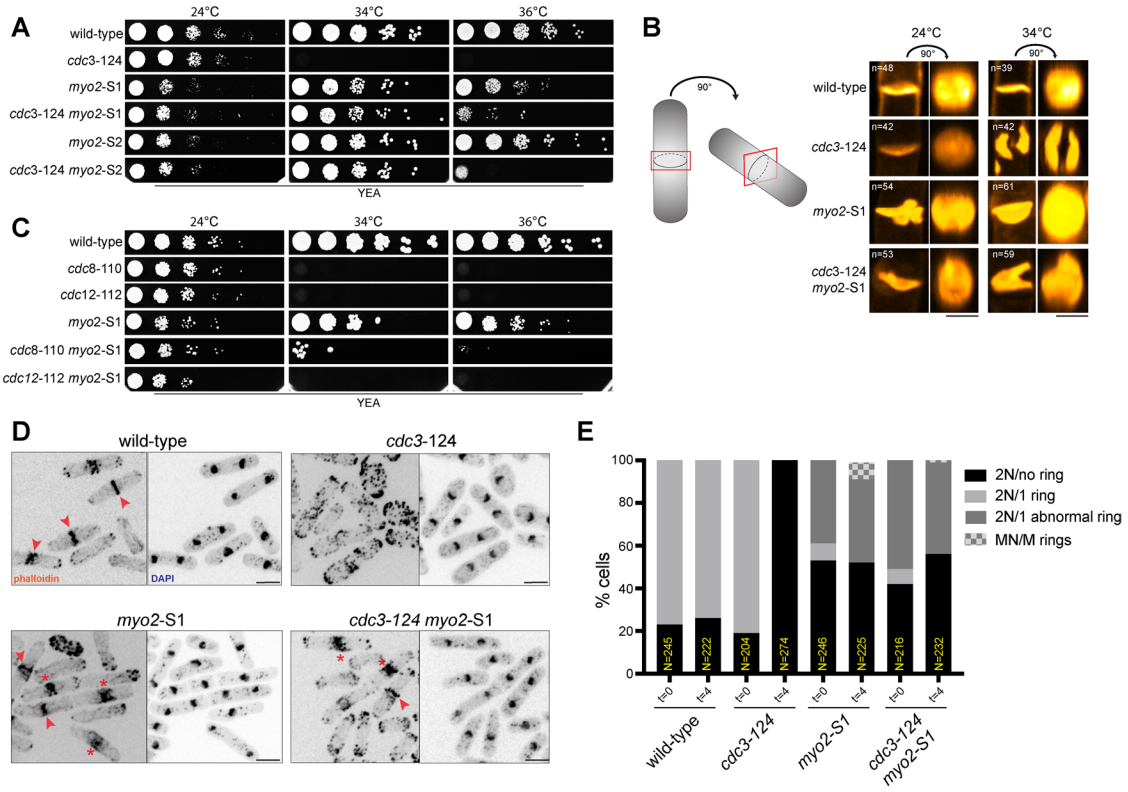


FIGURE 1: *myo2*-S1 suppresses the lethality of *cdc3*-124 at the nonpermissive temperature. (A) Tenfold serial dilutions of wild-type, *cdc3*-124, *myo2*-S1, *cdc3*-124 *myo2*-S1, *myo2*-S2, and *cdc3*-124 *myo2*-S2 were spotted onto YEA agar plates and grown for 3 d at 24, 34, and 36°C. (B) CW staining was used to visualize the septum of wild-type, *cdc3*-124, *myo2*-S1, and *cdc3*-124 *myo2*-S1 cells at 34°C. In the first column it is shown the acquired front view image of the septum, while in the second column it is displayed the face-on view of the septum, which was generated with Fiji software. Scale bar 3 µm. (C) Tenfold serial dilutions of wild-type, *cdc8*-110, *cdc12*-112, *myo2*-S1, *cdc8*-110 *myo2*-S1, and *cdc12*-112 *myo2*-S1 were spotted onto YEA agar plates and grown for 3 d at 24, 34, and 36°C. (D) Cells of the indicated genotypes were grown at 24°C and shifted for 4 h at 34°C and stained with CF633-phalloidin and DAPI. Arrows indicated normal AMRs while asterisks indicated abnormal rings. Scale bar 5 µm. (E) Quantification of CF633-phalloidin and DAPI staining in D of three independent experiments ($n = 3$). Cells with two nuclei were classified depending on the presence of no ring (2N/no ring), 1 normal ring (2N/1 ring), 1 abnormal ring (2N/abnormal ring), or multiple nuclei and rings (MN/M rings).

*cdc3*-124. Since *myo2*-S1 better suppressed the *cdc3*-124 defect, we characterized this mutant further.

The strains described above were stained with Calcofluor white (CW) to visualize the division septa. Whereas normal (or weakly defective) division septa that appeared as a disk in tilted images were detected at 24°C in all strains, disk-like complete septa were found in wild-type, *myo2*-S1, and *cdc3*-124 *myo2*-S1, but not in *cdc3*-124, at 34°C (Figure 1B). Instead, patches of septum material that did not create a barrier between the two daughters were observed in *cdc3*-124 at 34°C (Figure 1B). Although the septa detected in *cdc3*-124 *myo2*-S1 and *myo2*-S1 were complete and spanned the entire division site, they were nearly all abnormal in that they did not have a flat disk-like morphology observed in wild-type septa. Nevertheless, the fact that these septa were complete facilitated successful completion of cytokinesis in *cdc3*-124 *myo2*-S1 and *myo2*-S1.

Given the roles of Cdc12-formin in linear actin filament nucleation during cytokinesis (Chang *et al*., 1997; Kovar *et al*., 2003) and Cdc8-tropomyosin in stabilization of actin filaments in the AMR (Balasubramanian *et al*., 1992; Gunning *et al*., 2015; Khaitlina, 2015), we tested if the observed suppression was specific to Cdc3-profilin defects or if *myo2*-S1 also suppressed defects in *cdc12* and *cdc8*. To this end, we generated *cdc8*-110 *myo2*-S1 and *cdc12*-112 *myo2*-S1. We found that *cdc8*-110, but not *cdc12*-112, was suppressed at 34°C and tiny "pin-prick" colonies were observed even at 36°C (Figure 1C).

Next, we stained wild-type, *cdc3*-124, *myo2*-S1, and *cdc3*-124 *myo2*-S1 with CF633-phalloidin and DAPI to observe the actin cytoskeleton and nuclei (Figure 1, D and E). Whereas actin rings were not observed in *cdc3*-124, actin rings were observed in mitotic wild-type, *myo2*-S1, and *cdc3*-124 *myo2*-S1 (Figure 1D). The rings in *myo2*-S1 were more diffuse compared with those in wild type consistent with a role for Myo2 in AMR assembly. These experiments established that compromise of Myo2 function led to suppression of the defective AMR assembly, septum assembly, and colony formation in *cdc3*-124 (Figure 1E). The partial suppression of *cdc8*-110 by *myo2*-S1 (Figure 1C) suggested that *myo2*-S1 suppression is not specific to *cdc3*-124.

To investigate the mechanism of suppression of *cdc3*-124 by *myo2*-S1, as well as to characterize the phenotypic consequences of *myo2*-S1, we generated wild-type, *cdc3*-124, *myo2*-S1, and *cdc3*-124 *myo2*-S1 expressing Rlc1-3GFP (AMR marker) and mCherry-Atb2 (mitotic spindle marker). At 24°C, AMR assembly and contraction were indistinguishable in wild-type and *cdc3*-124 cells, whereas both processes were slightly slower in *myo2*-S1 and *cdc3*-124 *myo2*-S1 cells (Supplemental Figure S1, A and B). Ring assembly in wild type at 34°C took 17 ± 6.8 min and ring contraction took 18.7 ± 2.1 min (Figure 2, B and C). As expected, AMRs did not assemble in *cdc3*-124 cells, although Rlc1-3GFP accumulated first in nodes and then in multiple spots and bar-like structures (Figure 2A, class II). *myo2*-S1 showed a range of phenotypes pertaining to cytokinesis. First, in ~50% of the cells, ring assembly was delayed and took ~1.8 times longer (30.2 ± 4 min) than in wild-type cells and fully compacted rings were observed only in late mitotic cells (Figure 2, A, class I and class III, and B). Second, the remaining ~50% of the cells made abnormal actomyosin structures that did not compact into a ring (Figure 2A, class IV). Ring contraction was uniformly slower in cells that appeared to have normal rings (38.3 ± 6.9 min) (Figure 2C). Furthermore, ring contraction was asymmetric in nearly two-thirds of cells that appeared to have a normal looking ring (Figure 2A, class III). *cdc3*-124 *myo2*-S1 largely resembled *myo2*-S1 and rings of normal appearance were detected in ~42% of the cells and these rings took 26.2 ± 1.9 min to assemble, while the rest of the cells assembled Rlc1-3GFP bundles that did not compact into a ring (Figure 2, A and B). Ring contraction in *cdc3*-124 *myo2*-S1 cells was almost always asymmetric and the process took ~three times the time taken in wild type (56.3 ± 26.8 min) (Figure 2, A and C). These experiments established that *myo2*-S1 was compromised for both known physiological roles of Myo2.

### ATP-dependent contraction is slowed in AMRs isolated from *myo2*-S1

The mutated myosin allele, Myo2-S1, possesses a point mutation resulting in the replacement of Gly515 with an Asp in the L50 subdomain of Myo2 motor domain. G515D is located at the beginning of HR helix at the end of the activation loop (Varkuti *et al*., 2012). This glycine might play a role in the conformational flexibility of the activation loop, thereby contributing to the loop's orientation that facilitates actin binding. To understand the effect of the mutation, we analyzed the position equivalent to G515 in various myosin structures. In the cryoEM structure of myosin bound to actin filaments (5JLH), G515 was observed to be at the beginning of the activation loop that interacted with N-terminus of an actin monomer (Figure 3A). Modeling of the G515D mutation on myosin motor domain structure (1VOM) showed a salt bridge between the mutated Asp515 and the Arg509 residues (data not shown). Arg520 in *Caenorhabditis elegans* muscle myosin, corresponding to Lys510 in *S. pombe* Myo2, has been shown to be crucial for binding with the N-terminus of actin (Varkuti *et al*., 2012). Furthermore, Arg520 mutation affected the ATPase activity of myosin indicating that Arg520 interaction with actin is essential for motor domain function (Varkuti *et al*., 2012). In a sequence alignment of 237 nonredundant myosin sequences, glycine is highly conserved and a positively charged residue (at least one arginine or lysine) is a conserved feature of the activation loop (Figure 3B). Unavailability or misorientation of the positively charged side chain (K to R) to interact with actin in the G515D mutant (Myo2-S1) might weaken its interaction with actin, leading to abnormalities in ring assembly. Myo2-S1 may also affect the motor activity in the defective rings during contraction due to the absence of ATPase stimulation on actin interaction.

Given these considerations based on structural analysis of *myo2*-S1, we tested the biochemical properties of Myo2-S1, especially as it pertains with actin binding or motor activity. We were unable to purify this protein in sufficient quantities for biochemical studies. As an alternative, we used the permeabilized spheroplast assay, in which AMRs contract in an ATP- and Myosin II-dependent manner (Mishra *et al*., 2013). We prepared cell ghosts from wild-type, *myo2*-S1, and *cdc3*-124 *myo2*-S1 cells expressing Rlc1-3GFP that were grown at 24°C. We carried out two sets of experiments, one at 24°C (Supplemental Figure S2A) and the other at 34°C (Figure 4A, Supplemental Figure S2B, and Supplemental Movie S1). AMRs in wild-type ghosts contracted rapidly on ATP addition at 24°C (Supplemental Figure S2A and Figure 4C). However, AMRs became extremely unstable on introduction of the *myo2*-S1 mutation, suggesting that Myo2-S1 may interact weakly with actin causing the ring to be unstable (Supplemental Figure S2A). We therefore stabilized AMR by incubation of cell ghosts with the actin-stabilizer Jasplakinolide (Jasp) (Holzinger, 2009). We next treated Jasp-stabilized AMR in cell ghosts with ATP. As observed in the absence of Jasp, rings in wild-type ghosts contracted rapidly at 34°C (Figure 4, A and B and Supplemental Movie S1). However, even though AMRs were stably maintained in *myo2*-S1 and *cdc3*-124 *myo2*-S1, they either failed to contract or were very slow to contract (Figure 4, A and B, and Supplemental Movie S1). A similar trend was observed when

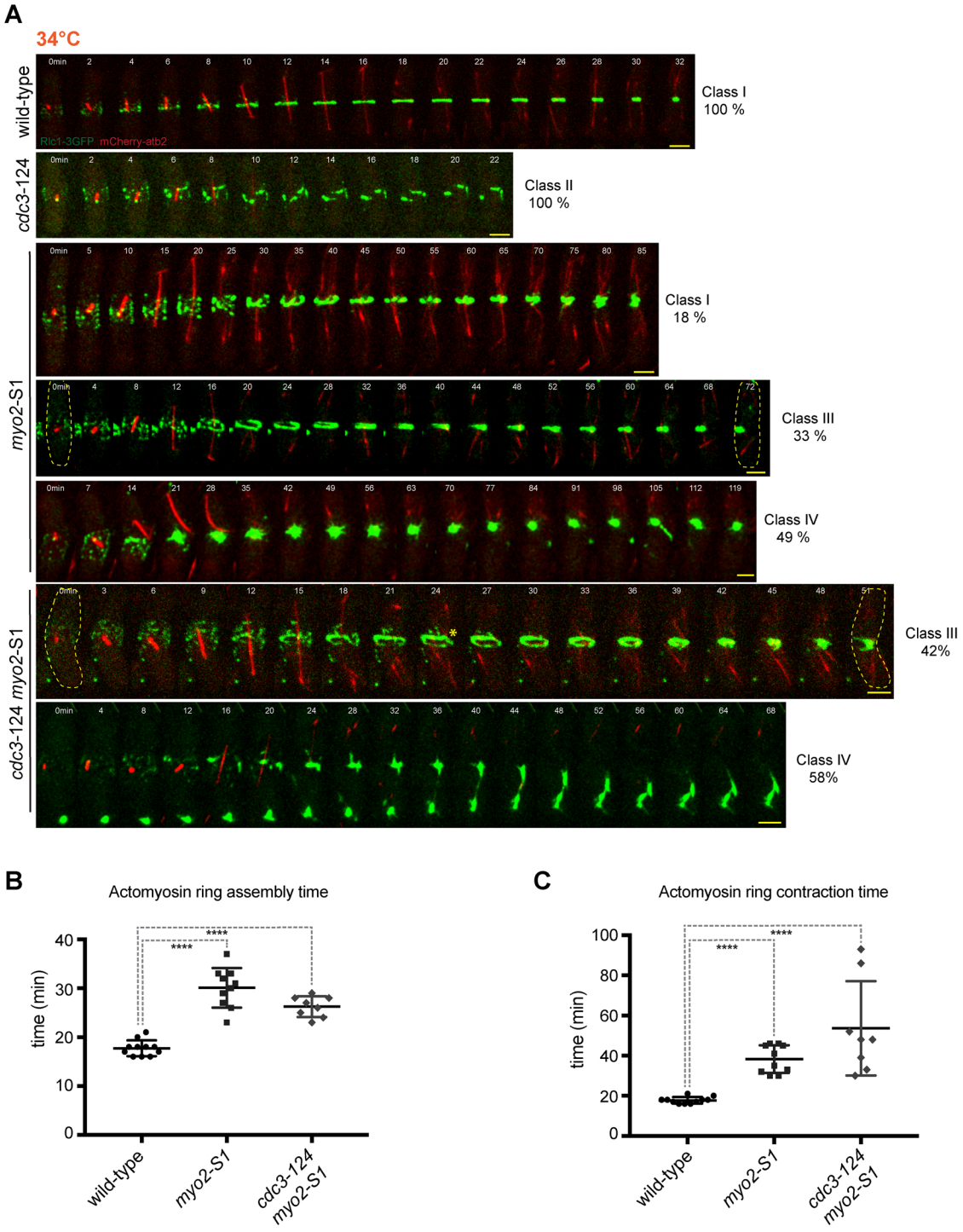


FIGURE 2: AMR assembly and contraction is partially restored in *myo2*-S1 and *cdc3*-124 *myo2*-S1 at 34°C. (A) Time-lapse series of strains of the indicated genotypes expressing Rlc1-3GFP and mCherry-Atb2. Cells were grown at 24°C and shifted 3 h at 34°C before being imaged at 34°C. More than 20 cells were imaged and quantified for each strain. On the side of each montage it is indicated the percentage of the different cytokinetic behaviors categorized into class I (normal AMR), class II (failed AMR assembly), class III (normal AMR assembly and asymmetrical AMR contraction), and class IV (abnormal AMR structures). Images shown are maximum-intensity projections of Z-stacks. Time indicated in minutes. Scale bars 3 µm. (B) Quantification of the time necessary for AMR assembly of class I and class III cells imaged in A. Statistical significance: Student's test (****$p < 0.0001$). Error bars represent SD. (C) Quantification of the time necessary for AMR contraction of class I and class III cells imaged in A. Statistical significance: Student's test (****$p < 0.0001$). Error bars represent SD.

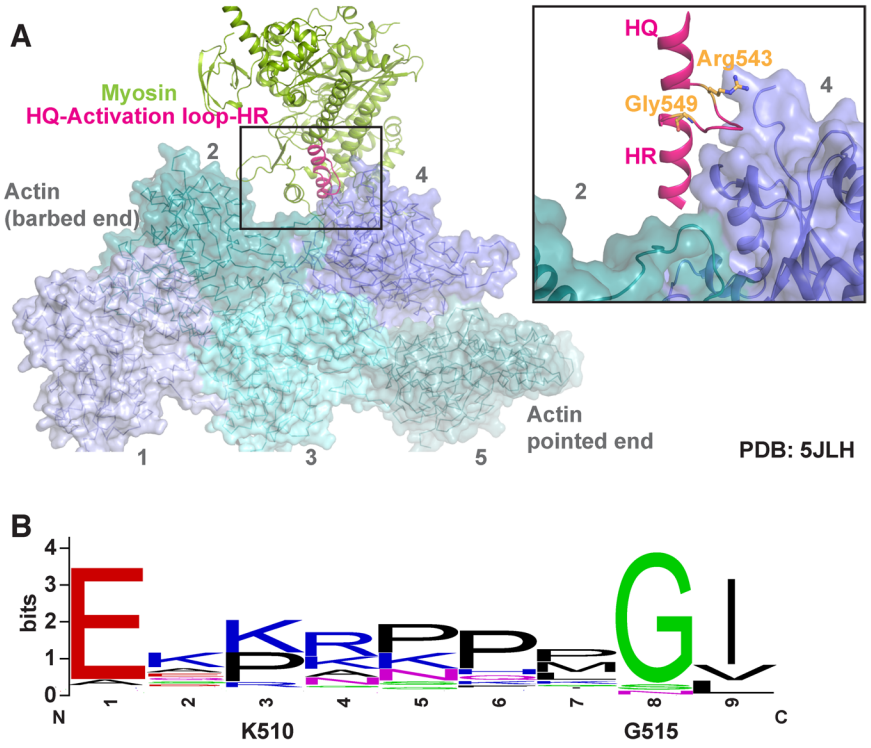


FIGURE 3: Structural basis of *S. pombe* Myo2-S1 (G515D) mutation. (A) Gly515 in *S. pombe* Myo2 (equivalent to Gly549 of human myosin 14 in the actomyosin complex structure of PDB ID: 5JLH) is positioned at the boundary of the activation loop at the myosin-actin interface. Inset shows the zoomed view of the interaction between the activation loop and the N-terminus of actin protomer. Gly549 and Arg543, corresponding to Gly515 and Lys510 of *S. pombe* Myo2, are shown in stick representation. The figure was generated using PyMol. (B) Conservation of Gly515 and Lys510 depicted on a sequence logo representation. The figure was generated using WebLogo (Crooks *et al.*, 2004) using a sequence alignment of 237 nonredundant myosin sequences aligned using ClustalO (Sievers *et al.*, 2011; Sievers and Higgins, 2018). The sequence corresponding to the activation loop was selected using JalView (Waterhouse *et al.*, 2009).

Jasp-stabilized *myo2*-S1, and *cdc3*-124 *myo2*-S1 ghosts were incubated with ATP even at 24°C (Figure 4C), similar to previous observations with *myo2*-E1 ghosts (Mishra *et al.*, 2013; Palani *et al.*, 2017). In addition, we found that Jasp-stabilized AMRs in *cdc3*-124 *myo2*-S2 ghosts also underwent very slow ATP-dependent contraction at 34°C (Supplemental Figure S2, B and C) and at 24°C (Supplemental Figure S2D). These observations established that loss of Myosin II motor activity strongly correlated with the suppression of AMR assembly/stability defects in *cdc3*-124.

### *myo2*-S1 suppresses direct pharmacological perturbation of the actin cytoskeleton

Previous work has shown that Myosin II can break actin filaments in vitro both by stretching or by buckling (Murrell and Gardel, 2012; Vogel *et al.*, 2013) due to its motor activity. We have shown that Myosin II mutants defective in ATP-dependent contraction suppress defects caused by partial loss of key proteins contributing to the assembly/stability of actin filaments in the AMR. We reasoned that shorter or unstable actin filaments may be protected for longer periods in the *cdc3*-124 *myo2*-S1, *cdc8*-110 *myo2*-S1, and *cdc3*-124 *myo2*-S2 mutants, contributing to the observed suppression. We therefore tested if direct pharmacological perturbation of actin cables and AMRs by treatment with low doses of LatA (Ayscough *et al.*, 1997) can be reversed by compromise of Myo2. Previously, we have shown that treatment of wild-type cells with low doses of LatA (~0.25 µM) leads to cytokinesis defects (Mishra *et al.*, 2004). We plated serial dilutions of wild type, *cdc3*-124, *myo2*-S1, and *cdc3*-124 *myo2*-S1 with a series of doses of LatA and incubated these at 30 and 34°C (Figure 5A). Wild-type cells were capable of robust colony formation up to 0.25 µM LatA, but did not form colonies at 0.375 µM LatA (Figure 5A). Consistent with a role for Cdc3-profilin in actin filament assembly in the cytokinetic ring, *cdc3*-124 mutants were hypersensitive to 0.25 µM LatA. Interestingly, *myo2*-S1 was able to form colonies up to 0.375 µM LatA (Figure 5A), establishing that compromise of Myo2 function reverses the deleterious effects caused by actin perturbation. *cdc3*-124 *myo2*-S1 also formed colonies at 30°C at 0.375 µM LatA, although at 34°C, this strain only grew on plates containing 0.125 µM LatA (Figure 5A). The inability of the *cdc3*-124 to form colonies at and above 0.25 µM LatA potentially reflects an enhanced actin cytoskeletal defect due to the additive effect of loss of Cdc3 and LatA. CF633-Phalloidin staining of liquid cultures of the four strains showed that actin cables, rings, and patches were present at 0 time point in all four strains (Figure 5,B and C). After a 3-h incubation in 0.375 µM LatA, actin patches were observed in all four strains. However, actin cables/rings were not detected in wild type or *cdc3*-124 but were clearly detected in *myo2*-S1 and *cdc3*-124 *myo2*-S1 (Figure 5, B and C). It is unclear if the observed cablelike structures in *myo2*-S1 and *cdc3*-124 *myo2*-S1 were interphase cables or improperly organized AMRs. Notwithstanding, collectively, these experiments established that partial genetic or pharmacological perturbation of formin-generated actin structures can be suppressed by motor activity-defective Myo2.

In this study we provide evidence for a role for Myosin II in actin filament disassembly through the use of genetic and in vitro analyses and structural modeling. Previous work has shown that single actin filaments and networks of actin filaments are broken and disassembled by Myosin II through buckling (Murrell and Gardel, 2012; Vogel *et al.*, 2013). Previous work in *Schizosaccharomyces japonicus* has shown that actin filaments in isolated cytokinetic rings break into clusters in a Myosin II-dependent manner (Chew *et al.*, 2017). Our work may provide in vivo evidence in fission yeast for a role for Myosin II in actin filament disassembly and turnover, consistent with the work in mammalian cells (Murthy and Wadsworth, 2005; Wilson *et al.*, 2010). It is possible that formin-generated actin filaments are short and unstable in profilin and tropomyosin mutants and on exposure to low doses of LatA. In this case, compromise of Myosin II, which normally destabilizes actin filaments, rescues the instability of actin filaments and, in turn, the cytokinesis defects. It is possible that in the SCPR mechanism of cytokinesis (Vavylonis *et al.*, 2008), actin filaments at the division site are broken by both cofilin and Myosin II and that our work provides evidence for Myosin II-based breakage of actin filaments at the division site.

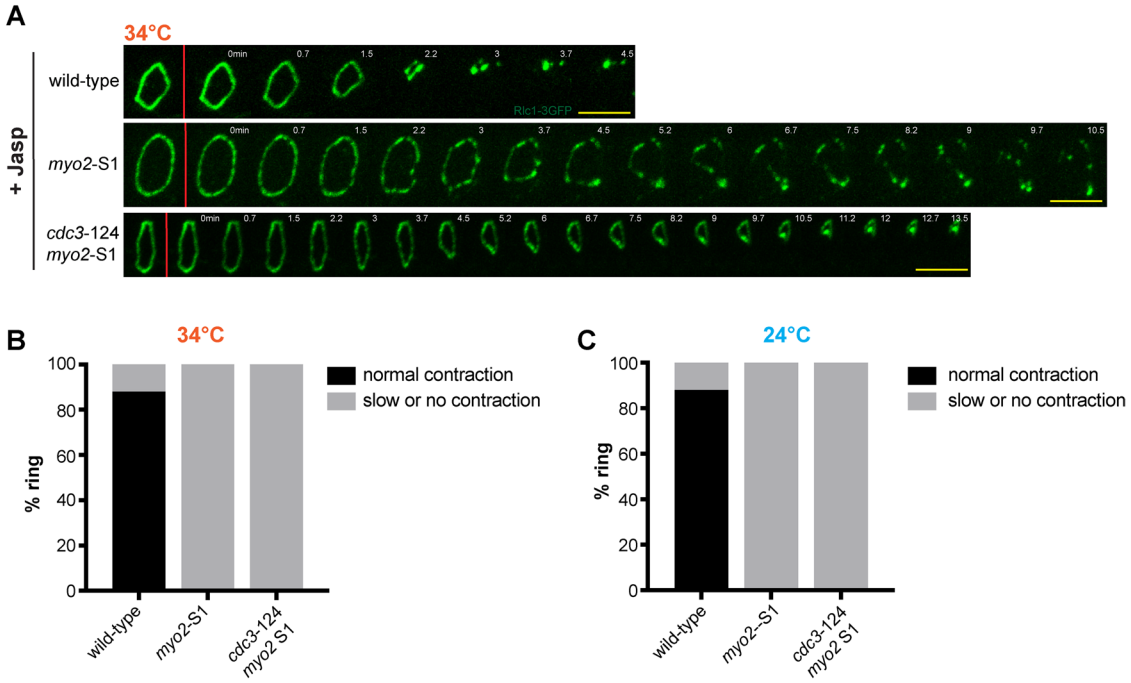


FIGURE 4: AMR isolated from *myo2*-S1 and *cdc3*-124 *myo2*-S1 cells do not undergo ATP-dependent contraction. (A) AMR were prepared from wild-type ($n = 17$), *myo2*-S1 ($n = 14$), and *cdc3*-124 *myo2*-S1 ($n = 20$) cells grown at 24°C in the presence of 20 µM Jasp. Isolated rings were shifted 15 min at 34°C before proceeding with imaging. Ring contraction experiments were performed at 34°C and contraction was activated by the addition of 0.5 mM ATP (indicated by the red bar). Myosin regulatory light chain (Rlc1-3GFP) was used as a marker protein to visualize AMR. Images shown are maximum intensity projections of Z-stacks. Time indicated in minutes. Scale bar 5 µm. (B) Percentage of rings that either contracted normally or presented slow/no contraction of strains imaged at 34°C illustrated in A. (C) Percentage of rings that either contracted normally or presented slow/no contraction of strains imaged at 24°C illustrated in A.

## MATERIALS AND METHODS

### Yeast genetics and culture methods

Cells were grown and cultured at 24°C in yeast extract medium (YES) as described previously (Moreno *et al.*, 1991). The presence of designated mutations on each used strain has been verified by PCR and DNA sequencing. Yeast strains used in the study are listed in Supplemental Table S1.

### PFA fixation and fluorescence microscopy

*S. pombe* cells, growing at 24°C in YES medium, were either fixed in mid-log phases or shifted to 34°C for 3–4 h before fixation. Cells were fixed in a 4% paraformaldehyde solution for 12 min at room temperature and, after two washes with 1× phosphate-buffered saline (PBS), permeabilized with 1% Triton X-100 for 10 min. Cells were washed twice with 1× PBS and stained with either DAPI (4′,6-diamidino-2-phenylindole, from Life Technologies) for the visualization of the nucleus or CF633-Phalloidin (CF633, from Biotium) to visualize actin structures. To visualize the septa, fixed *S. pombe* cells were directly incubated with CW (Sigma-Aldrich). Still images were acquired using a spinning disk confocal microscope (specifications described in *Live-cell imaging* below) and processed using imaging software Fiji. Face-on views of septa were generated using the Reslice function in Fiji, with a spacing of 0.15 µm, and the resulting images were then maximum intensity projected.

### Live-cell imaging

Mid-log phase cells were grown at 24°C in YES medium and, when necessary, shifted at 34°C for 3–4 h before imaging acquisition of live cells in a temperature-controlled incubation chamber. Time-lapse images were acquired for 3–4 h using a spinning disk confocal microscope (Andor Revolution XD imaging system, equipped with a 100× oil immersion 1.45 NA Nikon Plan Apo lambda, and a confocal unit Yokogawa CSU-X1, EMCCD detector [Andor iXON] and Andor iQ acquisition software). Cells were imaged in a CellASIC microfluidic yeast plates (Y04C and D size), where 15 Z-stacks of 0.5-µm thickness images were acquired at 1-min intervals for Rlc1-3GFP (myosin regulatory light chain, used as AMR marker) and mCherry-Atb2 (alpha tubulin 2, used as cell cycle marker). PRISM 6.0 software (GraphPad) was used for quantification and the statistical significance was determined using Student's *t* test (****$p < 0.0001$).

### Isolation of AMRs and ATP-dependent contraction

AMRs were isolated as described previously (Mishra *et al.*, 2013; Huang *et al.*, 2016). Time-lapse imaging of Rlc1-3GFP was acquired as described before in CellASIC microfluidic yeast plates (Y04D), where 21 Z-stacks of 0.5-µm thickness images were acquired while treating the cells with 0.5 mM ATP, either at 24°C or after shifting 15 min the isolated ring at 34°C. Fiji imaging software was used to process the acquired images, obtaining the maximum intensity projection of the Z-stacks.

### Drug treatments in cells and isolated AMRs

YES agar plates in Figure 5A were prepared by the addition of different concentrations of LatA (Enzo Life Sciences), where cells were successively being spotted at 10-fold serial dilutions. For the treatment in Figure 5B, cells were grown in liquid YES medium at 24°C and successively shifted at 34°C in the presence of 0.375 µM LatA in the medium for 3 h before fixation. Isolated AMRs were

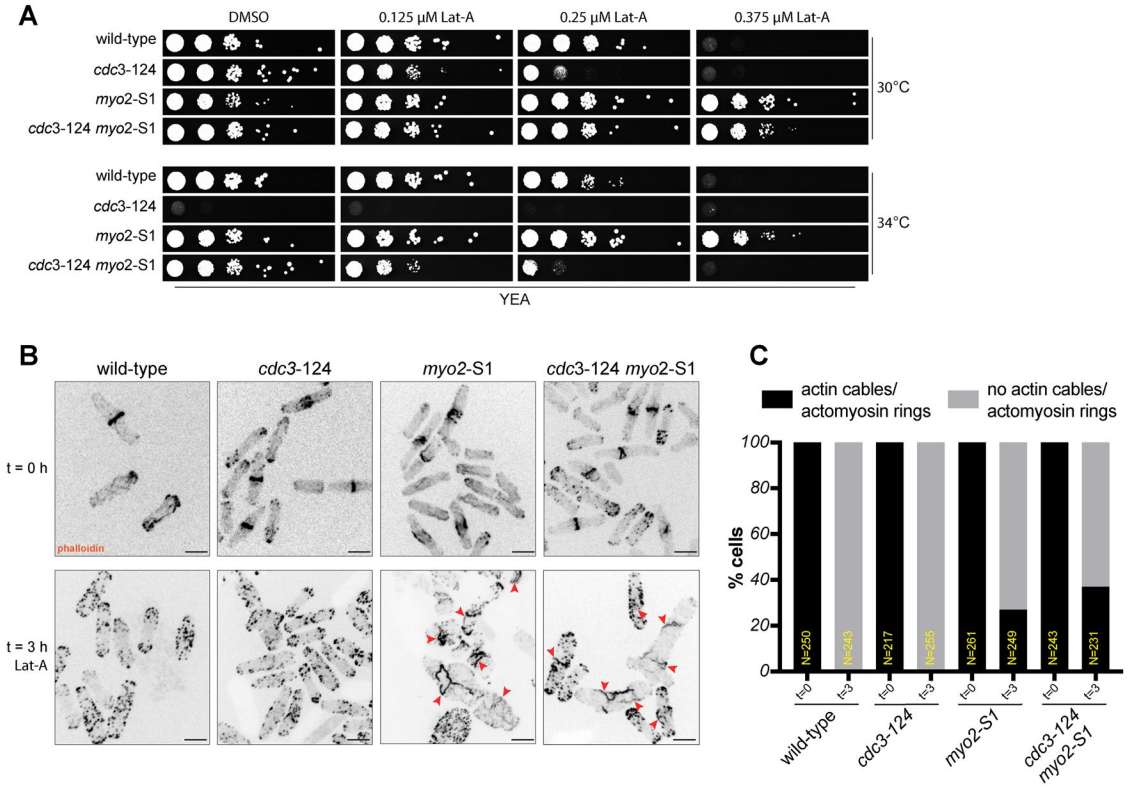


FIGURE 5: *myo2*-S1 suppresses perturbations of actin induced by LatA. (A) Tenfold serial dilutions of wild-type, *cdc3*-124, *myo2*-S1, and *cdc3*-124 *myo2*-S1 cells were spotted onto YEA agar plates containing different concentrations of LatA and grown for 3 d at 34 and 36°C. (B) Cells were grown at 24°C and shifted for 3 h at 34°C in the presence of 0.375 µM of LatA before PFA fixation. CF633-phalloidin was used to visualize actin structures of wild-type, *cdc3*-124, *myo2*-S1, and *cdc3*-124 *myo2*-S1 cells. Arrows indicated the presence of actin cables. Scale bar 5 µm. (C) Quantification of the presence of actin cables or AMR structure detected with CF633-phalloidin staining in B of three independent experiments ($n = 3$).

treated, when indicated, with Jasp (Enzo Life Sciences) by the addition of the drug to the isolated rings at the final concentration of 20 µM.

## ACKNOWLEDGMENTS

This work was funded by the Wellcome Trust (WT101885MA) and ERC (GA 671083—ACTOMYOSIN RING) to M.K.B. P.G. was supported by research grant from the SERB Women Excellence Award and Collaborative Research Grant from CEFIPRA (Indo-French Centre for Promotion of Advanced Research). S.S.J. acknowledges INSPIRE for fellowship. We thank Bernardo Chapa-y-Lazo for help with image analysis.

## REFERENCES

Ayscough KR, Stryker J, Pokala N, Sanders M, Crews P, Drubin DG (1997). High rates of actin filament turnover in budding yeast and roles for actin in establishment and maintenance of cell polarity revealed using the actin inhibitor latrunculin-A. J Cell Biol 137, 399–416.

Balasubramanian MK, Feoktistova A, McCollum D, Gould KL (1996). Fission yeast Sop2p: a novel and evolutionarily conserved protein that interacts with Arp3p and modulates profilin function. EMBO J 15, 6426–6437.

Balasubramanian MK, Helfman DM, Hemmingsen SM (1992). A new tropomyosin essential for cytokinesis in the fission yeast S. pombe. Nature 360, 84–87.

Balasubramanian MK, Hirani BR, Burke JD, Gould KL (1994). The Schizosaccharomyces pombe cdc3+ gene encodes a profilin essential for cytokinesis. J Cell Biol 125, 1289–1301.

Balasubramanian MK, McCollum D, Chang L, Wong KC, Naqvi NI, He X, Sazer S, Gould KL (1998). Isolation and characterization of new fission yeast cytokinesis mutants. Genetics 149, 1265–1275.

Bezanilla M, Forsburg SL, Pollard TD (1997). Identification of a second myosin-II in Schizosaccharomyces pombe: Myp2p is conditionally required for cytokinesis. Mol Biol Cell 8, 2693–2705.

Cai C, Henty-Ridilla JL, Szymanski DB, Staiger CJ (2014). Arabidopsis myosin XI: a motor rules the tracks. Plant Physiol 166, 1359–1370.

Chang F, Drubin D, Nurse P (1997). cdc12p, a protein required for cytokinesis in fission yeast, is a component of the cell division ring and interacts with profilin. J Cell Biol 137, 169–182.

Cheffings TH, Burroughs NJ, Balasubramanian MK (2016). Actomyosin ring formation and tension generation in eukaryotic cytokinesis. Curr Biol 26, R719–R737.

Chew TG, Huang J, Palani S, Sommese R, Kamnev A, Hatano T, Gu Y, Oliferenko S, Sivaramakrishnan S, Balasubramanian MK (2017). Actin turnover maintains actin filament homeostasis during cytokinetic ring contraction. J Cell Biol 216, 2657–2667.

Chiou JG, Balasubramanian MK, Lew DJ (2017). Cell polarity in yeast. Annu Rev Cell Dev Biol 33, 77–101.

Crooks GE, Hon G, Chandonia JM, Brenner SE (2004). WebLogo: a sequence logo generator. Genome Res 14, 1188–1190.

Feierbach B, Chang F (2001). Roles of the fission yeast formin for3p in cell polarity, actin cable formation and symmetric cell division. Curr Biol 11, 1656–1665.

Gunning PW, Hardeman EC, Lappalainen P, Mulvihill DP (2015). Tropomyosin - master regulator of actin filament function in the cytoskeleton. J Cell Sci 128, 2965–2974.

Henty-Ridilla JL, Li J, Blanchoin L, Staiger CJ (2013). Actin dynamics in the cortical array of plant cells. Curr Opin Plant Biol 16, 678–687.

Holtzman DA, Wertman KF, Drubin DG (1994). Mapping actin surfaces required for functional interactions in vivo. J Cell Biol 126, 423–432.

Holzinger A (2009). Jasplakinolide: an actin-specific reagent that promotes actin polymerization. Methods Mol Biol 586, 71–87.

Huang J, Mishra M, Palani S, Chew TG, Balasubramanian MK (2016). Isolation of cytokinetic actomyosin rings from Saccharomyces

cerevisiae and Schizosaccharomyces pombe. Methods Mol Biol 1369, 125–136.
Khaitlina SY (2015). Tropomyosin as a regulator of actin dynamics. Int Rev Cell Mol Biol 318, 255–291.
Kitayama C, Sugimoto A, Yamamoto M (1997). Type II myosin heavy chain encoded by the myo2 gene composes the contractile ring during cytokinesis in Schizosaccharomyces pombe. J Cell Biol 137, 1309–1319.
Kovar DR, Kuhn JR, Tichy AL, Pollard TD (2003). The fission yeast cytokinesis formin Cdc12p is a barbed end actin filament capping protein gated by profilin. J Cell Biol 161, 875–887.
Kovar DR, Sirotkin V, Lord M (2011). Three's company: the fission yeast actin cytoskeleton. Trends Cell Biol 21, 177–187.
Lee SH, Dominguez R (2010). Regulation of actin cytoskeleton dynamics in cells. Mol Cells 29, 311–325.
Liu HP, Bretscher A (1989). Disruption of the single tropomyosin gene in yeast results in the disappearance of actin cables from the cytoskeleton. Cell 57, 233–242.
May KM, Watts FZ, Jones N, Hyams JS (1997). Type II myosin involved in cytokinesis in the fission yeast, Schizosaccharomyces pombe. Cell Motil Cytoskeleton 38, 385–396.
McCollum D, Feoktistova A, Morphew M, Balasubramanian M, Gould KL (1996). The Schizosaccharomyces pombe actin-related protein, Arp3, is a component of the cortical actin cytoskeleton and interacts with profilin. EMBO J 15, 6438–6446.
Mishra M, Karagiannis J, Trautmann S, Wang H, McCollum D, Balasubramanian MK (2004). The Clp1p/Flp1p phosphatase ensures completion of cytokinesis in response to minor perturbation of the cell division machinery in Schizosaccharomyces pombe. J Cell Sci 117, 3897–3910.
Mishra M, Kashiwazaki J, Takagi T, Srinivasan R, Huang Y, Balasubramanian MK, Mabuchi I (2013). In vitro contraction of cytokinetic ring depends on myosin II but not on actin dynamics. Nat Cell Biol 15, 853–859.
Misu S, Takebayashi M, Miyamoto K (2017). Nuclear actin in development and transcriptional reprogramming. Front Genet 8, 27.
Moreno S, Klar A, Nurse P (1991). Molecular genetic analysis of fission yeast Schizosaccharomyces pombe. Methods Enzymol 194, 795–823.
Motegi F, Nakano K, Kitayama C, Yamamoto M, Mabuchi I (1997). Identification of Myo3, a second type-II myosin heavy chain in the fission yeast Schizosaccharomyces pombe. FEBS Lett 420, 161–166.
Murrell MP, Gardel ML (2012). F-actin buckling coordinates contractility and severing in a biomimetic actomyosin cortex. Proc Natl Acad Sci USA 109, 20820–20825.
Murthy K, Wadsworth P (2005). Myosin-II-dependent localization and dynamics of F-actin during cytokinesis. Curr Biol 15, 724–731.
Nakano K, Kuwayama H, Kawasaki M, Numata O, Takaine M (2010). GMF is an evolutionarily developed Adf/cofilin-super family protein involved in the Arp2/3 complex-mediated organization of the actin cytoskeleton. Cytoskeleton (Hoboken) 67, 373–382.
Nakano K, Mabuchi I (2006). Actin-depolymerizing protein Adf1 is required for formation and maintenance of the contractile ring during cytokinesis in fission yeast. Mol Biol Cell 17, 1933–1945.
Palani S, Chew TG, Ramanujam S, Kamnev A, Harne S, Chapa YLB, Hogg R, Sevugan M, Mishra M, Gayathri P, Balasubramanian MK (2017). Motor activity dependent and independent functions of Myosin II contribute to actomyosin ring assembly and contraction in Schizosaccharomyces pombe. Curr Biol 27, 751–757.
Pavlov D, Muhlrad A, Cooper J, Wear M, Reisler E (2007). Actin filament severing by cofilin. J Mol Biol 365, 1350–1358.
Pelham RJ, Chang F (2002). Actin dynamics in the contractile ring during cytokinesis in fission yeast. Nature 419, 82–86.
Pelham RJ Jr, Chang F (2001). Role of actin polymerization and actin cables in actin-patch movement in Schizosaccharomyces pombe. Nat Cell Biol 3, 235–244.
Pollard TD, Wu JQ (2010). Understanding cytokinesis: lessons from fission yeast. Nat Rev Mol Cell Biol 11, 149–155.
Rottner K, Faix J, Bogdan S, Linder S, Kerkhoff E (2017). Actin assembly mechanisms at a glance. J Cell Sci 130, 3427–3435.
Sievers F, Higgins DG (2018). Clustal Omega for making accurate alignments of many protein sequences. Protein Sci 27, 135–145.
Sievers F, Wilm A, Dineen D, Gibson TJ, Karplus K, Li W, Lopez R, McWilliam H, Remmert M, Soding J, *et al*. (2011). Fast, scalable generation of high-quality protein multiple sequence alignments using Clustal Omega. Mol Syst Biol 7, 539.
Sirotkin V, Berro J, Macmillan K, Zhao L, Pollard TD (2010). Quantitative analysis of the mechanism of endocytic actin patch assembly and disassembly in fission yeast. Mol Biol Cell 21, 2894–2904.
Skruber K, Read TA, Vitriol EA (2018). Reconsidering an active role for G-actin in cytoskeletal regulation. J Cell Sci 131.
Staiger CJ, Sheahan MB, Khurana P, Wang X, McCurdy DW, Blanchoin L (2009). Actin filament dynamics are dominated by rapid growth and severing activity in the Arabidopsis cortical array. J Cell Biol 184, 269–280.
Varkuti BH, Yang Z, Kintses B, Erdelyi P, Bardos-Nagy I, Kovacs AL, Hari P, Kellermayer M, Vellai T, Malnasi-Csizmadia A (2012). A novel actin binding site of myosin required for effective muscle contraction. Nat Struct Mol Biol 19, 299–306.
Vavylonis D, Wu JQ, Hao S, O'Shaughnessy B, Pollard TD (2008). Assembly mechanism of the contractile ring for cytokinesis by fission yeast. Science 319, 97–100.
Vogel SK, Petrasek Z, Heinemann F, Schwille P (2013). Myosin motors fragment and compact membrane-bound actin filaments. Elife 2, e00116.
Waterhouse AM, Procter JB, Martin DM, Clamp M, Barton GJ (2009). Jalview Version 2—a multiple sequence alignment editor and analysis workbench. Bioinformatics 25, 1189–1191.
Wertman KF, Drubin DG, Botstein D (1992). Systematic mutational analysis of the yeast ACT1 gene. Genetics 132, 337–350.
Wilson CA, Tsuchida MA, Allen GM, Barnhart EL, Applegate KT, Yam PT, Ji L, Keren K, Danuser G, Theriot JA (2010). Myosin II contributes to cell-scale actin network treadmilling through network disassembly. Nature 465, 373–377.
Wong KC, Naqvi NI, Iino Y, Yamamoto M, Balasubramanian MK (2000). Fission yeast Rng3p: an UCS-domain protein that mediates myosin II assembly during cytokinesis. J Cell Sci 113 (Pt 13), 2421–2432.
Wu JQ, Bahler J, Pringle JR (2001). Roles of a fimbrin and an alpha-actinin-like protein in fission yeast cell polarization and cytokinesis. Mol Biol Cell 12, 1061–1077.